Electronic Supplementary Material (ESI) for Nanoscale.
This journal is © The Royal Society of Chemistry 2020
Electronic Supplementary Material (ESI) for Nanoscale.
This journal is © The Royal Society of Chemistry 2020

Electronic Supplementary Information (ESI)

Large-Area 2D $PtTe_2$/Silicon Vertical-Junction Devices with Ultrafast and High-Sensitivity Photodetection and Photovoltaic Enhancement by Water Droplet

Mashiyat Sumaiya Shawkat,[a, b] Tanvir Ahmed Chowdhury,[c] Hee-Suk Chung,[d] Shahid Sattar,[e] Tae-Jun Ko,[a] J. Andreas Larsson,[e] and Yeonwoong Jung*[a, b, f]

[a] *NanoScience Technology Center, University of Central Florida, Orlando, Florida 32826, USA. E-mail: yeonwoong.jung@ucf.edu*
[b] *Department of Electrical and Computer Engineering, University of Central Florida, Orlando, Florida 32816, USA.*
[c] *Department of Mechanical and Aerospace Engineering, University of Central Florida, Orlando, Florida 32816, USA.*
[d] *Analytical Research Division, Korea Basic Science Institute, Jeonju 54907, South Korea.*
[e] *Applied Physics, Division of Materials Science, Department of Engineering Sciences and Mathematics, Luleå University of Technology, Luleå SE 97187, Sweden.*
[f] *Department of Materials Science and Engineering, University of Central Florida, Orlando, Florida 32816, USA.*

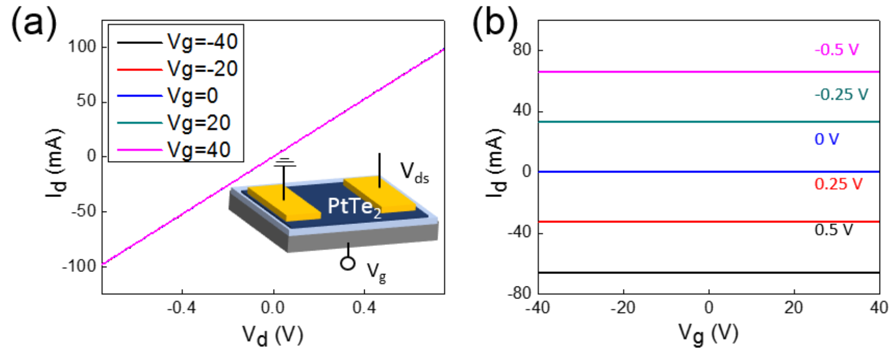

Figure S1. (a) Drain current (I_d) – voltage (V_d) output characteristics with varying gate voltage (V_g) in the back-gated configuration corresponding to the inset device schematic. The results show a negligible FET gate response, confirming the strongly metallic nature of the 2D $PtTe_2$ layers. (b) I_d–V_g transfer characteristics of the same FET, further confirming V_g-independent metallic transport.

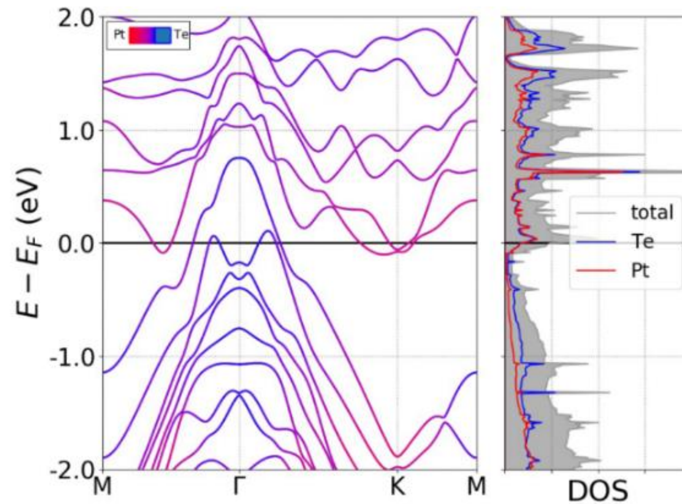

Figure S2. DFT calculations showing the electronic band structure (left) and the atom-projected density of states (DOS)(right) of 2D $PtTe_2$ tri-layers. Metallic dispersion characteristics are observed, which is attributed to the strong interlayer coupling within the 2D layers due to the pronounced hybridization of Pt and Te atomic orbitals around the Fermi level.

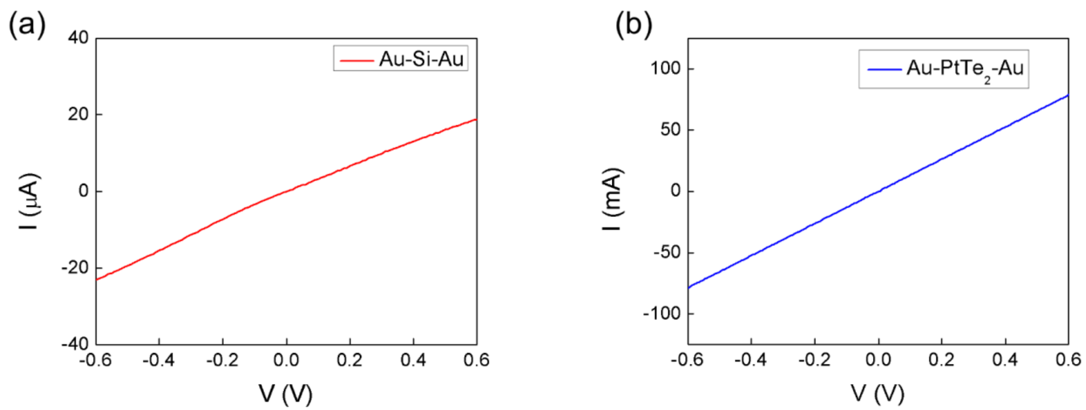

Figure S3. IV characteristics from (a) only-p-Si and (b) only-$PtTe_2$ using Au electrodes.

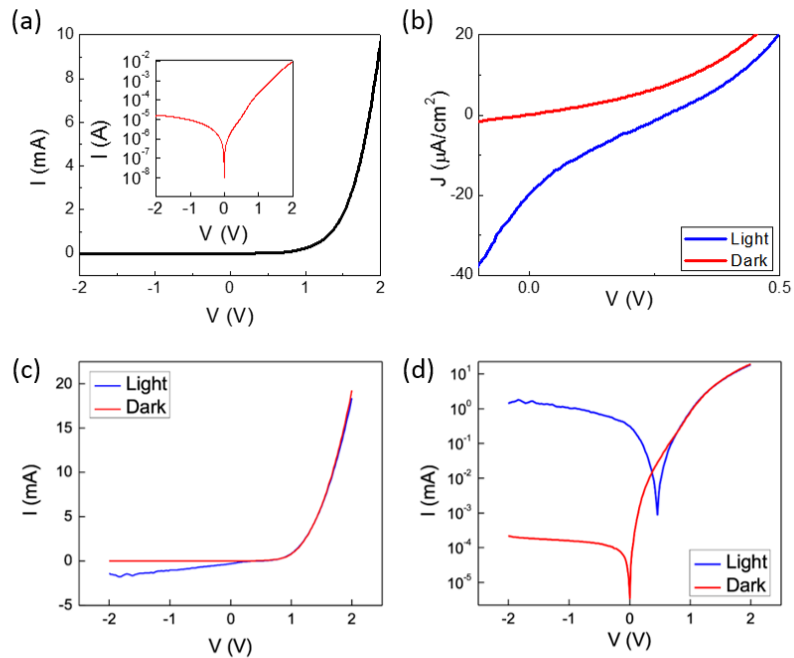

Figure S4. (a-b): Electrical and photovoltaic characteristics of a device prepared with Pt of ~0.3 nm. (a) I-V curve in a linear scale as well as its corresponding semi-log plot (inset). (b) J-V curves in dark (red) and under illumination (blue). (c-d): Electrical and photovoltaic characteristics of a device prepared with Pt of ~13.5 nm. I-V curves in (c) linear- and (d) semi-log scales. For both cases, the extracted PCE is < 1 %.

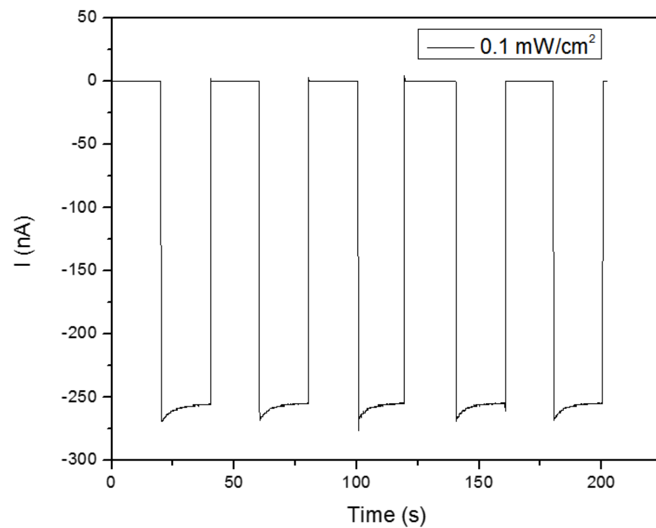

Figure S5. Photo-responsiveness at zero bias under the low illumination intensity of 0.1 mW/cm^2.

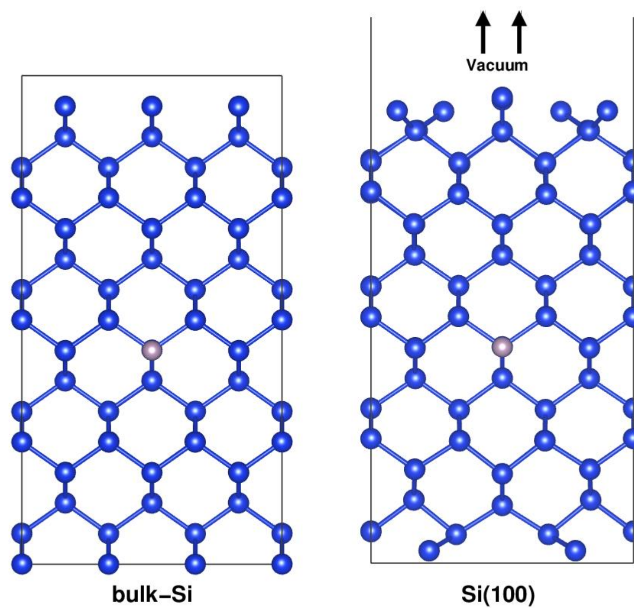

Figure S6. Side view of Si (100) bulk and slab configurations having one of 144 Si atoms replaced by a boron atom to obtain p-doping.

Computational method: We performed first-principles calculations using density functional theory (DFT) adopting the projector augmented wave method[1, 2] as implemented in the Vienna Ab-initio Simulation Package (VASP)[3]. In our simulations, we used trilayer $PtTe_2$ as a representative system to model few layer $PtTe_2$. For the exchange-correlation potential, we employed the non-local optB86b-vdW density functional[4, 5] to account for the van der Waals interactions between the layers with a plane-wave energy cutoff of 420 eV. A gamma-centered Monkhorst-Pack 16×16×1 k-mesh was used for self-consistent calculation. For the iterative solution of the Kohn-Sham equations, an energy convergence of 10^{-6} eV and a force convergence of 10^{-3} eV/Å was achieved. Moreover, due to the constituent heavy elements in $PtTe_2$, the effects of spin-orbit coupling were taken into account in our calculations. We also used a 15 Å thick layer of vacuum on top of few layer $PtTe_2$ to exclude any spurious interaction between periodic images in the out-of-plane direction as three-dimensional periodic boundary conditions were applied. The Raman spectrum in Figure 1(b) was obtained by calculating the derivative of the macroscopic dielectric tensor with respect to the mode coordinates using VASP assisted python package.[6] To obtain the work function of few layer $PtTe_2$, we converged the electrostatic potential with respect to the vacuum level (E_{vac}) and calculated the planar average potential in the out-of-plane (001) direction. For the Si work function computation, a 3×3×2 supercell of Si(100) using bulk and non-passivated slab configurations - both with 144 Si atoms - was used by adopting the electrostatic potential lineup method[7], whereas the experimental bandgap of Si (1.10 eV) was used to derive the conduction band offset. The simulation of p type Si was achieved by replacing one Si atom with a boron (B), which results in less than 1% doping concentration.

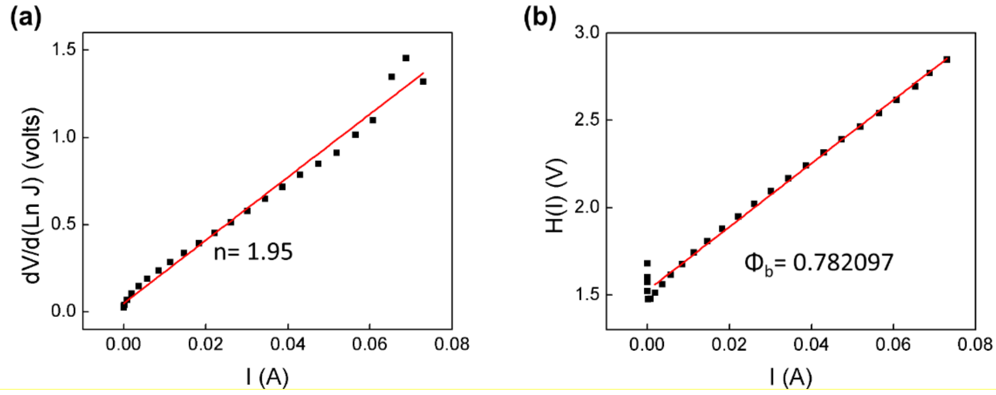

Figure S7. Plots of (a) *dV/d(Ln J)* vs *I*, and (b) *H(I)* vs *I* for 2D $PtTe_2$ layers prepared with Pt film of ~4.5 nm.

Extraction of Schottky barrier diode parameters:

According to the thermionic emission theory,[7,8] the current, *I*, through a Schottky diode can be expressed as

$$I = I_0 \, exp(\frac{q(V-IR_S)}{nKT}) \tag{1}$$

Furthermore, I_o is the reverse saturation current which can be modelled as:

$$I_0 = AA^{**}T^2 exp(\frac{-q\Phi_B}{kT}) \tag{2}$$

Here, *q* is the charge of an electron, A^{**} is the Richardson constant for Si, and *A* is the active diode surface area, *T* is the absolute temperature, *k* is the Boltzmann constant, R_s is the series resistance, and *V* is the voltage applied across the diode. The diode equation can be re-expressed as;[9]

$$\frac{dV}{d(\ln J)} = IR_s + n(\frac{kT}{q}) \tag{3}$$

Where *J* = *I/A*,

$$IR_S + n\Phi_B \; = V - n\left(\frac{kT}{q}\right) \ln\left(\frac{I}{AA^{**}T^2}\right) \tag{4}$$

The ideality factor, *n*, can be extracted from the linear plot of *dV/d(Ln J*) in Eq. (S3) and it is identified to be ~1.95 from Figure S7(a). Also, an auxiliary equation is defined as

$$H(I) = V - n\left(\frac{kT}{q}\right)\ln\left(\frac{I}{AA^{**}T^2}\right) \quad (5)$$

and

$$H(I) = IR_s + n\Phi_B \quad (6)$$

Using the linearity of the plot of *H(I)* vs. *I* from Eq. (S6), the Schottky barrier height, Φ_B, can be extracted from the y-axis intercept of the plot. Figure S7(b) presents a plot of *H(I)* vs. *I* for the 2D $PtTe_2$ layers prepared with Pt film of ~4.5 nm, which yields height Φ_B ~0.78 eV.

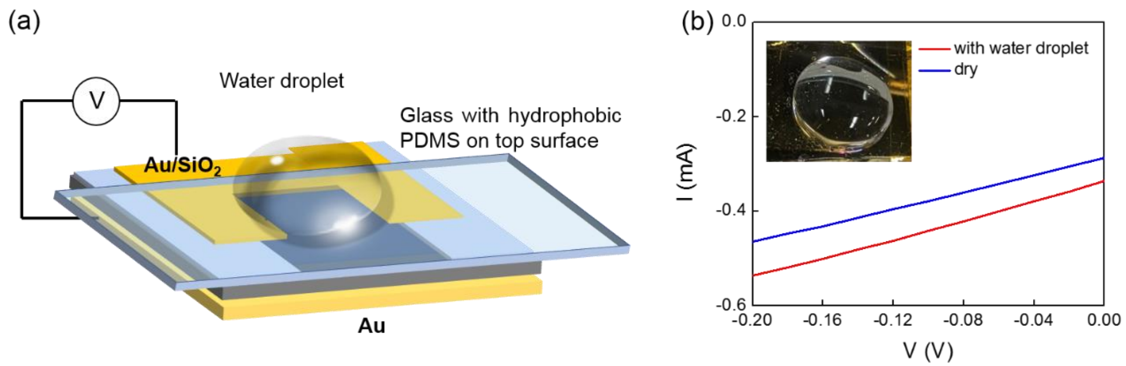

Figure S8. (a) Schematic of measurement set-up. A glass slide coated with a hydrophobic polydimethylsiloxane (PDMS) film is placed on the active area of $PtTe_2$/Si and the light is illuminated from the top side of the integrated water droplet. (b) I-V characteristics under identical illumination with (red) and without (blue) water droplet integration.

Table 1: Comparison of key parameters of this study with previously reported 2D/3D Photodetectors

Device Structure	Fabrication Method	Active Area	Measurement condition	EQE (%)	Photoresponsivity ($mA\ /W^{-1}$)	Detectivity (Jones)	Response Time Rise time (τ_r)/Fall time (τ_f)	Reference
$MoTe_2$/ Si	Pulsed Laser Deposition	0.42 cm^2	V=0V, λ=980 nm	24	190	$6.8\ \times 10^{13}$	150 ns/350 ns	[10]
$PtSe_2$/Si	Chemical Vapor Deposition	0.0126 cm^2	V=0V, λ=808 nm	80	520	$3.26\ \times\ 10^{13}$	55.3/170.5 µs	[11]
$PtSe_2$/Ge	Chemical Vapor Deposition	0.06 cm^2	V=0V, λ=1550 nm	48.2%	602	$6.31\ \times\ 10^{11}$	7.42/16.71 µs	[12]
$PdSe_2$/Perovskite	Chemical Vapor Deposition	0.08 cm^2	V=0V, λ=808 nm	$\sim 50\%$	313	$2.72\times\ 10^{13}$	3.5/4 µs	[13]
$PdSe_2$/Si	Chemical Vapor Deposition	0.01 cm^2	V=0, λ=780 nm	-	300.2	$1\times\ 10^{13}$	38/44 µs	[14]
Graphene /Silicon	Chemical Vapor Deposition	0.1 cm^2	V=0V, λ= 890 nm	$\sim 57\%$	730	4.08×10^{13}	320/75 µs	[15]
GaSe/Si	MBE	-	V=0V, λ= 532.8 nm	~23.6 %	100	-	60/20 µs	[16]
$PtTe_2$/Si	Chemical Vapor Deposition	0.5	V=0V, λ= 625 nm	42.2 %.	213	$2.66\times\ 10^{13}$	1.68/1.58 µs	This work

References for Electronic Suplementary Information

1. P. E. Blöchl, *Phys. Rev. B*, 1994, **50**, 17953-17979.
2. G. Kresse and J. Furthmüller, *Phys. Rev. B*, 1996, **54**, 11169-11186.
3. G. Kresse and D. Joubert, *Phys. Rev. B*, 1999, **59**, 1758-1775.
4. J. Klimeš, D. R. Bowler and A. Michaelides, *J. Phys.: Condens. Matter*, 2009, **22**, 022201.
5. J. Klimeš, D. R. Bowler and A. Michaelides, *Phys. Rev. B*, 2011, **83**, 195131.
6. A. Fonari and S. Stauffer, *vasp_raman.py*, https://github.com/raman-sc/VASP/, 2013.
7. M. Peressi, N. Binggeli and A. Baldereschi, *J. Phys. D: Appl. Phys.*, 1998, **31**, 1273-1299.
8. E. H. Rhoderick, *IEE Proceedings I - Solid-State and Electron Devices*, 1982, **129**, 1.
9. S. K. Cheung and N. W. Cheung, *Appl. Phys. Lett.*, 1986, **49**, 85-87.
10. Z. Lu, Y. Xu, Y. Yu, K. Xu, J. Mao, G. Xu, Y. Ma, D. Wu and J. Jie, *Adv. Funct. Mater.*, 2020, **30**, 1907951.
11. C. Xie, L. Zeng, Z. Zhang, Y.-H. Tsang, L. Luo and J.-H. Lee, *Nanoscale*, 2018, **10**, 15285-15293.
12. L. Wang, J.-J. Li, Q. Fan, Z.-F. Huang, Y.-C. Lu, C. Xie, C.-Y. Wu and L.-B. Luo, *J. Mater. Chem. C*, 2019, **7**, 5019-5027.
13. L.-H. Zeng, Q.-M. Chen, Z.-X. Zhang, D. Wu, H. Yuan, Y.-Y. Li, W. Qarony, S. P. Lau, L.-B. Luo and Y. H. Tsang, *Adv. Sci.*, 2019, **6**, 1901134.
14. L.-H. Zeng, D. Wu, S.-H. Lin, C. Xie, H.-Y. Yuan, W. Lu, S. P. Lau, Y. Chai, L.-B. Luo, Z.-J. Li and Y. H. Tsang, *Adv. Funct. Mater.*, 2019, **29**, 1806878.
15. X. Li, M. Zhu, M. Du, Z. Lv, L. Zhang, Y. Li, Y. Yang, T. Yang, X. Li, K. Wang, H. Zhu and Y. Fang, *Small*, 2016, **12**, 595-601.
16. X. Yuan, L. Tang, S. Liu, P. Wang, Z. Chen, C. Zhang, Y. Liu, W. Wang, Y. Zou, C. Liu, N. Guo, J. Zou, P. Zhou, W. Hu and F. Xiu, *Nano Lett.*, 2015, **15**, 3571-3577.